Effect of humidified water vapor on heat balance management in a proton exchange membrane fuel cell stack

Zhichun Liu[1],[*],[†], Jun Shen[1], Houchang Pei[1], Zhengkai Tu[2],[‡],[§], Jun Wang[2], Zhongmin Wan[3],[¶],[‖] and Wei Liu[1]

[1]School of Energy and Power Engineering, Huazhong University of Science and Technology, Wuhan 430074, China
[2]State Key Laboratory of Advanced Technology for Materials Synthesis and Processing, Wuhan University of Technology, Wuhan 430070, China
[3]School of Physics and Electronic Engineering, Hunan Institute of Science and Technology, Yueyang 414006, China

SUMMARY

Thermal management has been considered as one of the most important issues for the operation of proton exchange membrane fuel cells (PEMFCs). Phase change affects the performance and even the heat balance of the stack during operation. A 46 single cell PEM stack with anode and cathode humidification is developed to investigate, both theoretically and experimentally, the effect of phase change on the heat generation and removal characteristics of the stack. The results show that the heat removed by the coolant water is greater than that generated by the electrochemistry reaction, and heat released due to the phase change of water vapor cannot be neglected. Heat generated in the stack can be removed completely by the coolant water, which need to be forced cooling for recycling use when the current density reaches $1000\,\mathrm{mA\cdot cm^{-2}}$. The arithmetic product of the specific heat capacity and mass of the stack can be used as a novel criterion to evaluate the validity of the heat balance in the system. The exothermic reaction is very fast in the stack, which consequently requires bipolar plates with high heat conductivity coefficient to improve the temperature uniformity at the elevated operational current density. Copyright © 2014 John Wiley & Sons, Ltd.

KEY WORDS

proton exchange membrane fuel cell; phase change; heat balance; criterion

Correspondence

*Zhichun Liu, School of Energy and Power Engineering, Huazhong University of Science and Technology, Wuhan 430074, China.
[†]E-mail: zcliu@hust.edu.cn
[‡]Zhengkai Tu, State Key Laboratory of Advanced Technology for Materials Synthesis and Processing, Wuhan University of Technology, Wuhan 430070, China.
[§]E-mail: tzklq@whut.edu.cn
[¶]Zhongmin Wan, School of Physics and Electronic Engineering, Hunan Institute of Science and Technology, Yueyang 414006, China.
[‖]E-mail: zhongminwan@sohu.com

1. INTRODUCTION

As one of the promising clean energy sources, proton exchange membrane fuel cell (PEMFC), also known as polymer electrolyte membrane fuel cell, has attracted increasing research interest because of its high power density and wide range of applications including automotive and stationary area [1–4]. Restricted by the properties of the electrolyte material, small temperature variations and an operating temperature below 80 °C [5,6] are required for the state-of-the-art PEMFC to improve the efficiency, reliability, and durability of the membrane electrode assembly (MEA) [7]. During

operation, an amount of waste heat comparable to its electric power output is produced and the operation temperature will increase continuously if the waste heat is not rejected efficiently from the fuel cell [8]. As a consequence, thermal management is critical in PEMFC, especially in high temperature PEMFC [9]. Furthermore, coupled with thermal management another critical requirement for PEMFC is to maintain a high water content in the electrolyte to ensure reasonable ionic conductivity [10]. Wan *et al.* [11] and Yu *et al.* [12] have carried out some research on water management, such as water recovery and air humidification by exhaust gas and water drainage aided by gravity. Water molecules must be continuously

supplied to prevent drying of the membrane which can lead to a dramatic decrease in ionic conductivity. The most commonly used technique is to humidify the reaction gases through humidifiers prior to flowing into the fuel cell. The water vapor with high enthalpy in the humidified gases causes a complex condensation process inside the cell. Accordingly, phase change coupled with water management will heavily impact both the performance and the heat balance of the fuel cell.

To accurately model the heat transfer process in PEM fuel cell, Ramousse *et al.* [13] discussed heat sources/sinks distribution in a single cell. They pointed out that water phase change was governed by both thermal and water distributions in the gas diffusion layer (GDL), and it could take place anywhere in the GDL. A fully coupled heat and mass transfer model is thus needed to identify the location/region of water condensation and evaporation. Park *et al.* [14,15] investigated the characteristics of liquid water removal from the GDL by reactant flow both numerically and experimentally. Unsteady two-phase simulation results indicated that liquid water could be effectively removed from the gas diffusion layer by the reactant flow, and the amount of pressure drop and contact angle were the key parameters which determined the initiation of the liquid water transport in the gas diffusion layer. Measuring unsteady pressure drop in a cell which had the GDL initially wet with liquid water revealed that the characteristics of liquid water removal were significantly affected by the thickness of GDL and reactant flow rate. And the simulation results were also compared with experimental data showing a good agreement. Zhou *et al.* [16] developed a water and thermal management model with phase change to simulate the mass and energy transfer in a PEM fuel cell. Their results showed that the humidification of both anode and cathode sides was an important factor influencing the performance of the PEM fuel cell. The humidification could also directly influence the amount of phase change and the heat balance in the fuel cell. Afshari *et al.* [17,18] proposed a two-dimensional, two-phase, non-isothermal, single-domain approach using coupled electrochemical kinetic model to investigate the heat transfer phenomena and water phase change effects on the thermal behavior of a PEM fuel cell. They found that phase change would have a subtle effect on the maximum temperature that appeared at the cell inlet when the inlet gas was partially humidified. When using the two phase model, the cell temperature in all regions was higher than that with single phase model due to the phase change occurring at the inlet. In addition, the amount and location of condensation in the GDL cathode was directly related to cell temperature, and the temperature distribution strongly affected the two-phase water transport. Okazaki *et al.* [19,20] proposed a two-phase non-isothermal model to investigate the spatial distribution of the phase-change rate of the interfacial mass transfer on the cathode side of a proton exchange membrane fuel cell (PEMFC). They also

discussed the temporal variation and spatial distribution of the phase-change rates at the cathode side of PEM fuel cell. It was found that phase change quickly responded the temperature and a steady condensation could be achieved in a short time inside the fuel cell. Yi *et al.* [21] developed a two-dimensional, non-isothermal model of a proton exchange membrane fuel cell, which included various modes of heat generation and depletion by reversible/irreversible heat release, ohmic heating, and phase change of water, to elucidate heat balance through the MEA. Ju *et al.* [22] used a three-dimensional, non-isothermal model to account rigorously for various heat generation mechanisms. They concluded that the thermal effect on PEM fuel cells becomes more critical at higher current density and/or lower gas diffusion layer thermal conductivity. Tang *et al.* [23] established a system-level dynamic model accounting for the phase change effect for PEMFC. This model could illustrate the complex transient behavior of temperature, gas flow, phase change in the anode and cathode channels, and membrane humidification. Their results showed that vapor in the cathode channel was more likely to be in the superheated state and phase change (condensation under large load current situation) could occur easily. On the contrary, phase change was less likely to occur if the inlet hydrogen was humidified with a high relative humidity value. Kim [24] investigated the effect of humidity and stoichiometry on the water saturation of PEM fuel cells based on the finite element method. The results showed that, whether the reactant on anode or cathode was sufficiently humidified, a lower RH of the left reactant would improve cell performance, and higher stoichiometry could enhanced the performance at a constant $RHa = 100\%$ and $RHc = 100\%$. Rasheed *et al.* [25] used a simple analytical transient model to consider the effects of boiling phase change in the cathode catalyst layer and cathode gas diffusion layer on thermal and water balance during the warm-up process of a high temperature of membrane fuel cell. The energy consumption due to boiling phase change was found to be negligible compared with external heating input rate, and boiling phase change would be also present for a significant period of time under typical operating conditions.

Above mentioned work [13–25] shows that the understanding of the phase change, water management, and heat balance plays an important role in the design of state-of-the-art PEMFC. Previous studies on phase change were mainly focused on its effect on temperature or the factor that influences the phase change, while few articles refer to the specific effect of heat balance. Although the heat lost in the by-product that resulted from the electrochemical reactions at the anode and cathode could be easily calculated [26], heat source caused by phase change and its effect on heat balance inside the stack has typically been neglected. In addition, the aforementioned research focused mainly on a small single cell or a specific section of fuel cell, such

as the flow channel or MEA, and there have been few studies on the effect of the phase change on the heat balance and the performance in a practical operated PEMFC stack. In this paper, a model of heat balance in a 46 single cell PEM stack with both 80% humidified hydrogen and oxygen gases is developed and the issues, in particular, the effect of phase change on the heat generation and removal, are analyzed both theoretically and experimentally.

2. THEORETICAL ANALYSIS

2.1. Heat generation in the stack

The chemical reaction process in fuel cell is expressed as,

$$H_2 + 1/2\,O_2 = H_2O(g) + \Delta\overline{h_f} \tag{1}$$
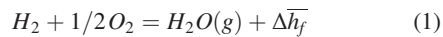
Equation (1) describes an exothermic reaction, where $\Delta\overline{h_f}$ is the change in molar enthalpy of formation. The value of $\Delta\overline{h_f}$ is approximately 242 kJ·mol^{-1} under the standard conditions (25 °C, 1 atm) with hydrogen completely combustion. However, the latent heat needed for the evaporation of the liquid water is approximately 42 kJ·mol^{-1}. Water exists as vapor or liquid phase depending on local temperature, pressure, and the water content in gas. Water vapor presented in the electrochemistry reaction is easy to condense into liquid [27], and the rate of heat generation with respect to the working current I can be expressed as [26,28]

$$Q = nI(1.25 - V_c) \tag{2}$$

where n is the number of cells, V_c is the average voltage during the operation process. Due to the order of 10^{-6} s of the time of electrochemical reaction, water produced in the exothermic reaction will exist in vapor state with tremendous heat releasing in such a short time. Then 1.25 V is the ideal open circuit voltage, only if the entire heat energy of combustion is converted to electrical energy, corresponding to the lower hydrogen heating value with water vapor generation.

2.2. Heat generated due to phase change

In general, liquid water will be produced in the cell when the water vapor pressure reaches its saturation value. The water used to humidify the reacting gas, which usually exists as vapor state with a high temperature and high enthalpy, will accelerate the condensation rate of the water vapor and introduce an additional heat source to the stack due to the exothermic process of phase change during the operation of the stack. The mass flow rate of water vapor at the inlet can be written as [11],

Anode

$$\dot{m}_{a,add} = \frac{n\lambda I}{2F} \cdot \frac{RH \cdot p_{sat}(T_{a,inlet})}{p_{a,inlet} - RH \cdot p_{sat}(T_{a,inlet})} M_{H_2O} \tag{3}$$

Cathode

$$\dot{m}_{c,add} = \frac{n\lambda I}{4F} \cdot \frac{RH \cdot p_{sat}(T_{c,inlet})}{p_{c,inlet} - RH \cdot p_{sat}(T_{c,inlet})} M_{H_2O} \tag{4}$$

where λ is the stoichiometry, F is the Faraday constant, $p_{a,inlet}$ and $p_{c,inlet}$ are the inlet pressure at the anode and cathode respectively, $T_{a,inlet}$ and $T_{c,inlet}$ are the inlet temperature at the anode and cathode, respectively, and $p_{sat}(T_{a,inlet})$ and $p_{sat}(T_{c,inlet})$ are the saturation water vapor pressure at the anode and cathode, respectively. In Eq. (4), RH is the relative humidity and M_{H_2O} is the water molecular weight.

The water vapor mass flow rates at the outlets of the anode and cathode are,

$$\dot{m}_{a,out} = (\lambda - 1)\frac{nI}{2F} \cdot \frac{RH \cdot p_{sat}(T_{a,outlet})}{p_{a,outlet} - RH \cdot p_{sat}(T_{a,outlet})} M_{H_2O} \tag{5}$$

and

$$\dot{m}_{c,out} = (\lambda - 1)\frac{nI}{4F} \cdot \frac{RH \cdot p_{sat}(T_{c,outlet})}{p_{c,outlet} - RH \cdot p_{sat}(T_{c,outlet})} M_{H_2O} \tag{6}$$

where $p_{a,outlet}$ and $p_{c,outlet}$ are the outlet pressure, $T_{a,outlet}$ and $T_{c,outlet}$ are the outlet temperature, and $p_{sat}(T_{a,outlet})$ and $p_{sat}(T_{c,outlet})$ are the saturation water vapor pressures at the anode and cathode, respectively.

The water vapor generation rate during the operation is,

$$\dot{m}_{gen,H_2O} = \frac{nI}{2F} M_{H_2O} \tag{7}$$

The liquid water flow rate due to phase change, including the net amount of water molecules transmitted in the membrane [29], can be expressed as,

$$\dot{m}_{l,H_2O} = \dot{m}_{a,add} - \dot{m}_{a,out} + \dot{m}_{c,add} - \dot{m}_{c,out} + \dot{m}_{gen,H_2O} \tag{8}$$

Heat generated due to phase change can be express as,

$$Q_{hg,water} = \dot{m}_{l,H_2O} L_{H_2O} \tag{9}$$

where L_{H_2O} is the latent heat of water, and the positive value indicates that the condensation process will heat up the stack.

2.3. Heat removal by the coolant water

Heat removal by the coolant water can be expressed as,

$$Q_c = C_{l,water} \dot{m}_{water} \left(T_{coolant\ water,out} - T_{coolant\ water,in} \right) \tag{10}$$

where $C_{l,water}$ and $\dot{m}_{water}$ are the specific heat and mass flow rate of the coolant water, respectively, and $T_{coolant\ water,in}$ and $T_{coolant\ water,out}$ are the inlet and outlet temperatures of the coolant water, respectively.

2.4. Heat balance in the stack

The heat removed by the exhaust stream and the heat loss from the stack surface to the ambient are negligible due to their low amount in the total heat removal. To study the heat balance behavior in the stack, a thermal balance coefficient ε is defined using stack thermal efficiency, which represents the ratio of heat removed by the coolant water to the actual heat generated in the stack. The balance coefficient can be written as,

$$
\begin{aligned}
\varepsilon &= \frac{Q_c}{Q + Q_{hg,water}} \\
&= \frac{C_{l,water} \dot{m}_{water} \left(T_{water,out} - T_{water,in} \right)}{nI(1.25 - V_c) + \dot{m}_{l,H_2O} L_{H_2O}}
\end{aligned} \tag{11}
$$

$\varepsilon < 1$ means poor cooling capacity of the coolant, while $\varepsilon > 1$ means excess cooling capacity, and $\varepsilon = 1$ is the equilibrium state.

3. EXPERIMENT

3.1. Experimental setup

The PEM fuel cells stack applied in this study is composed of 46 single cells using graphite plates as current collector. A straight-channel flow field similar to that used in Ref. [30] is applied in the single cell to ameliorate the water removal. The dimensions of the PEM fuel cell stack are listed in Table I. The MEAs consist of Nafion® 211 membrane in combination with platinum loadings of 0.4 mg·cm^{-2} per electrode. The performance tests of the stack were carried out on FCATS G500 purchased from Greenlight Innovation Company, Canada,

Table I. Dimensions of PEM fuel cell stack.

Single cell area of this stack (m^2)	200×10^{-4}
Flow field depth (m)	1.0×10^{-3}
Flow field width (m)	1.5×10^{-3}
Flow field ridge width (m)	1.5×10^{-3}
Gas diffusion layer thickness (m)	2.5×10^{-4}
PEM thickness (m)	2.5×10^{-5}
Catalyst layer thickness (m)	1.2×10^{-5}

which could be programmed precisely to control various operational parameters, including electronic load, gas flow rate or stoichiometry, dew point temperature, inlet/outlet pressure, inlet/outlet temperature, relative humidity (RH), and cell temperature. The schematic diagram of the test system for the PEM fuel cell stack is shown in Figure 1.

3.2. Experimental procedure

The whole experiment lasted more than 2 h and a half. To investigate the effect of the current density on the heat balance, current density was varied to be 500 mA·cm^{-2}, 600 mA·cm^{-2}, and 1000 mA·cm^{-2}, respectively during the experiment. To investigate the thermal characteristics during the temperature increasing process of the stack, the coolant water flow rate was maintained at 45 LPM (liter per minute) with a current density of 500 mA·cm^{-2}. The temperature decrease characteristics were studied by operating the cooling system at an elevated current density of 1000 mA·cm^{-2}. The effect of the coolant water flux on the heat removal ability was evaluated by changing the fluxes from 45 to 30 LPM with respect to a current density of 600 mA·cm^{-2}. To accurately evaluate the amount of liquid water produced by phase change during the experiment, T-type thermocouples and pressure sensors were placed at the inlet and outlet of the reaction gases
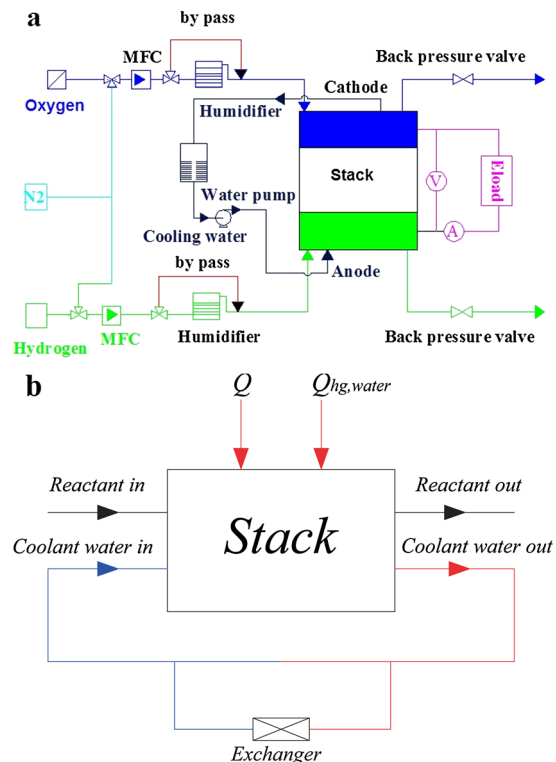
Figure 1. Schematic diagram of the test and heat removal system for PEMFC stack. (a) Test system; (b) heat removal system.

to monitor the gas temperature and pressure, respectively. The temperature variation of the coolant water was quantified by two thermocouples placed at the coolant water inlet and outlet, respectively. The evolution of temperature profile within the stack is measured by a representative thermocouple located at the middle of cell 23 in the stack showed in the Figure 2[31]. Except cell 23, cell 1, cell 11, and cell 46 were also similar design with 9 thermocouples located at. There were 38 thermocouples in all including thermocouples embedding between the GDL surfaces and coolant water inlet and outlet. The temperature range and accuracy of all the T-type thermocouples used in the measurement are $-200\,°C$ ~$350\,°C$, and $\pm0.1\,°C$, and the pressure range and accuracy of the pressure sensors are 0–300 kPa and ±0.1 kPa, respectively. Prior to the performance evaluation of the stack, the internal and external leakages of the reaction gases were checked, and the results were found to be acceptable. The fuel cell stack was pre-activated by increasing the current on the stack with 80% humidified H_2/O_2 for approximately 2 h before recording the polarization curves, which allowed us to evaluate the initial performance of the fuel cell stack. The detailed experimental conditions of the fuel cell stack are listed in Table II.

Air In
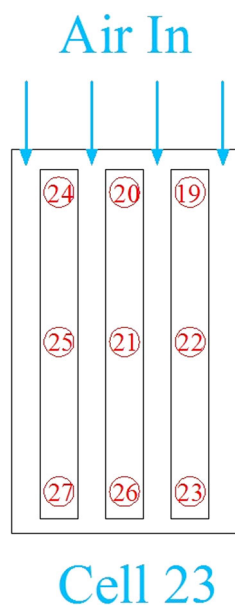
Cell 23

Figure 2. Schematic positions of the thermocouples located at Cell 23.

Table II. Testing conditions of the experiments.

Gas inlet temperature (K)	Anode/cathode = 343/343(70 °C)
Stoichiometry	Anode:cathode = 1.17:2.8
Dew point (K)	338 (65 °C)
Ambient temperature (K)	282 (9 °C)

4. RESULTS AND DISCUSSION

4.1. Evolution of temperature and pressure at the inlet and outlet of the stack

The evolution of the inlet/outlet temperature and pressure at different current densities is shown in Figure 3. The pressure differences of the three tested current densities in the anode are all less than 1×10^3 Pa. In the cathode they varied from 1.5×10^3 Pa, 3.5×10^3 Pa to 10.5×10^3 Pa corresponding to the current densities of 500 mA·cm^{-2}, 600 mA·cm^{-2}, and 1000 mA·cm^{-2}, respectively. The main reason for the dissimilar pressure differences is that the flow resistance of hydrogen is lower than that of the oxygen in the same flow channel due to the higher diffusion coefficient of hydrogen with less stoichiometry set at the anode. The increased pressure difference in the cathode is caused by the increased flow rate of the oxidant gas. In addition, the average flow velocities calculated from the inlet gas flow rate at the cathode were 0.33 m·s^{-1}, 0.40 m·s^{-1}, and 0.67 m·s^{-1}, respectively. The removal of water at such low velocities in the flow channel is due to both the gravitational effect and the use of the wider and deeper flow channel in the designed cell [30]. Compared with the set temperature of 70 °C, the fluctuation of the inlet temperature was within ±1 °C. The outlet temperature increased almost linearly with respect to time at current densities of 500 mA·cm^{-2} and 600 mA·cm^{-2}. The cooling system was opened to facilitate the temperature control at the current density 1000 mA·cm^{-2}. The average outlet temperature increase rate at 500 mA·cm^{-2} was 1.22 °C·min^{-1}, which decreased to 0.75 °C·min^{-1} at 600 mA·cm^{-2} and a coolant water flow rate of 45 LPM. The temperature of the coolant water was approximately 20 °C lower than the dew point of the inlet gas, which caused a greater temperature increase rate of approximately 0.80 °C·min^{-1} when the coolant water flow rate dropped to 30 LPM at 600 mA·cm^{-2}. As a result, the saturated water vapor with a high enthalpy in the reaction gases was condensed into liquid water inside the stack with a release of heat, which subsequently heated up the stack. The temperature difference between the stack and the inlet gas decreased with time and reduced to 2 °C when the coolant water flow rate was 30 LPM at 600 mA·cm^{-2}, indicating that little thermal energy was introduced into the stack due to phase change. In general, more heat would be generated during the electrochemistry reaction at a higher operating current density, which in turn caused the temperature difference between the single cell and the coolant water to increase rapidly [28]. Thus, cooling system was opened to remove excess heat sufficiently to maintain the operating temperature of the stack. The rates of increase and decease were almost equal (approximately 2.41 °C·min^{-1} at 1000 mA·cm^{-2}), as were the water condensation and evaporation rate during the cooling and heating process.
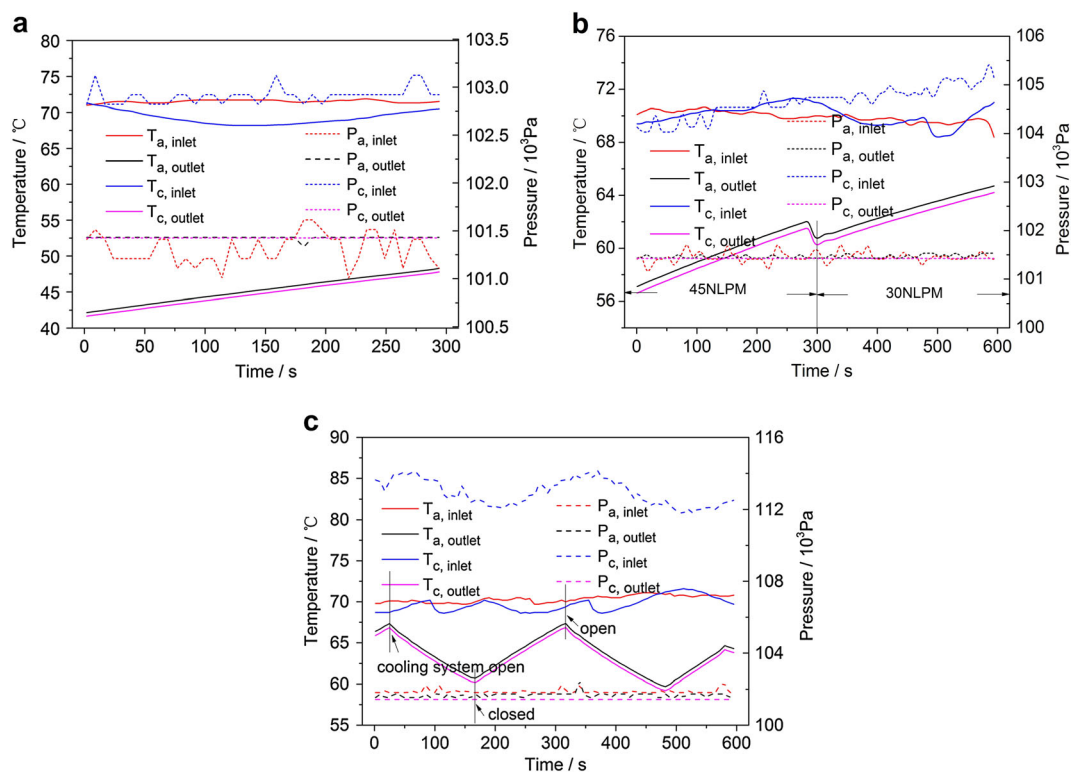
Figure 3. Temperature and pressure evolution in the inlet and outlet. (a) 500 mA·cm^{-2}. (b) 600 mA·cm^{-2}. (c) 1000 mA·cm^{-2}.

4.2. Rate of liquid water generation due to phase change

Although water in the inlet exists mainly in vapor phase, it moves out of the stack with the state of two phase flow. On the other hand, water would traverse the membrane under the coupled effects of electro-osmotic drag (EOD), back diffusion (BD), pressure driven hydraulic permeation (PDHE), and thermal-osmotic drag (TOD) [26]. Consequently, these factors made the measuring of the transport coefficient of water independently and accurately more difficult. In addition, water vapor may have condensed into liquid along the channel inside the stack, and liquid water would also evaporate into vapor in the elevated temperature section. To evaluate the rate of liquid water generation caused by phase change in the stack, we neglect the complex transport and phase change processes while focusing solely on the water vapor flow rate at the inlets and outlets. The inlet and outlet water vapor mass flow rates at the anode and cathode are shown in Figure 4(a) and (b), respectively. All mass flow rates increase with increasing current density. The amount of water at the inlet at the anode and cathode were almost same whereas water vapor mass flow rate at the cathode was greater than that at the outlet of the anode. Based on Eqs. (7) and (8), the water mass flow rates at the outlets were mainly determined by the stoichiometry when the pressure and temperature were almost equal (Figure 3) at the same current density. Stoichiometry has a significant effect on the phase change

process inside the stack. Figure 4(c) shows the amount of liquid estimated from Eq. (10). The average liquid water generation rates were 0.67×10^{-3} kg·s^{-1} and 1.18×10^{-3} kg·s^{-1} with respect to the current densities of 500 mA·cm^{-2} and 1000 mA·cm^{-2}, respectively. Therefore, the difference in the average liquid water generation rates was 0.51×10^{-3} kg·s^{-1}, significantly higher than the differences in the water vapor mass flow rate between the inlet and outlet, which were 0.11×10^{-3} kg·s^{-1} and 0.09×10^{-3} kg·s^{-1}, respectively at the elevated current density. The mass flow rate of the liquid water at a current density 1000 mA·cm^{-2} was less than double that at 500 mA·cm^{-2}, indicating that more of the water that was generated during the electrochemistry reaction was condensed into liquid inside the stack at 1000 mA·cm^{-2}. This is attributed to the increased temperature difference between the single cell and the coolant water with the rise of the current density. As a result, more water vapor was converted into liquid water because of the elevated sub-cooling, especially at high current density.

4.3. Heat removed by the coolant water

The heat generated in the stack is removed by the coolant water. The heat exchange rates of the coolant water at different current densities are shown in Figure 5(a), (b), and (c). The inlet and outlet temperature of the coolant water varied almost linearly with increasing or decreasing current density. The average temperature difference of the coolant
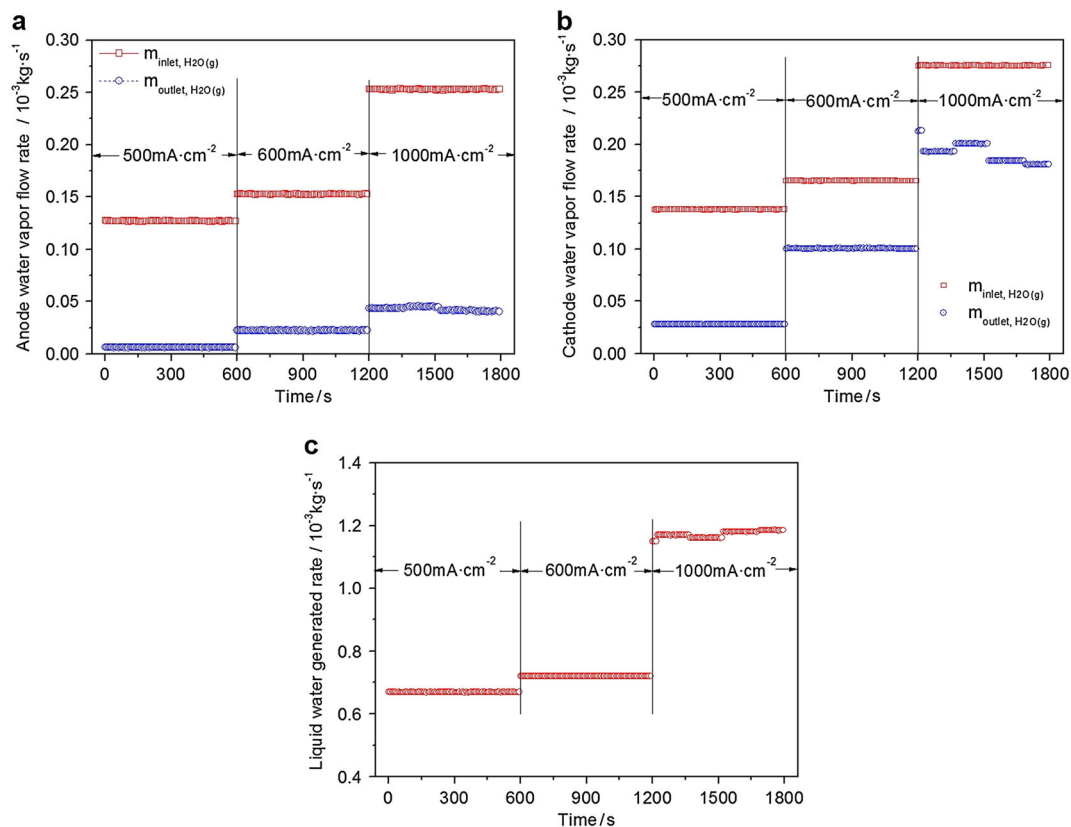
Figure 4. Rate of liquid water generation due to phase change. (a) Water vapor at anode. (b) Water vapor at cathode. (c) Liquid water generated in the stack.
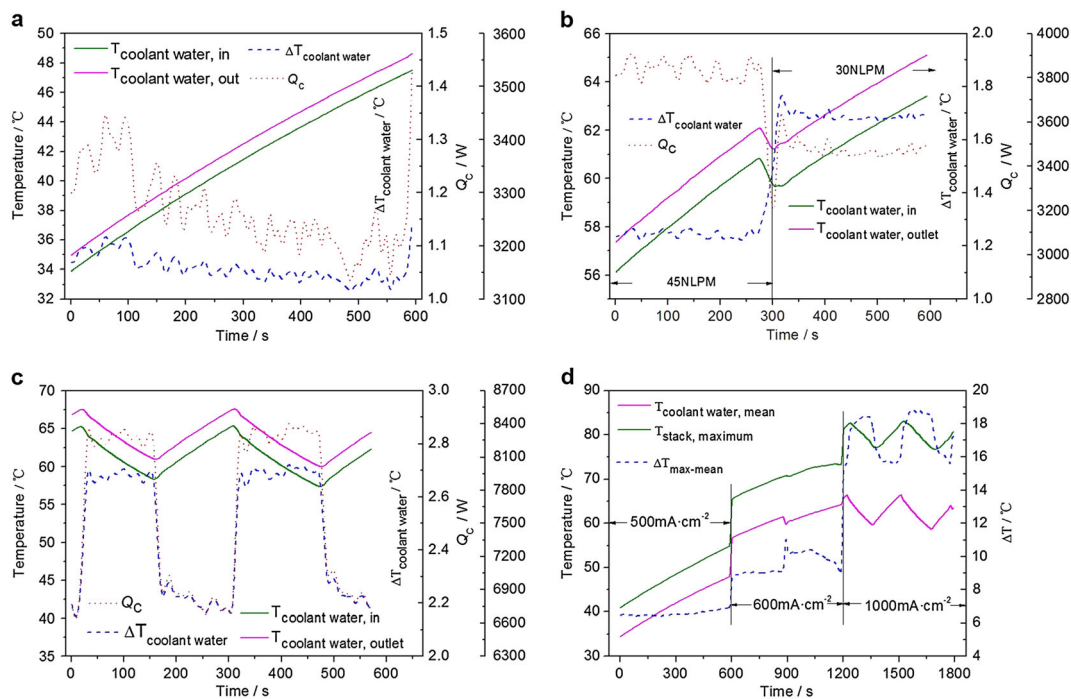
Figure 5. Heat removed by the coolant water. (a) 500 mA·cm^{-2}. (b) 600 mA·cm^{-2}. (c) 1000 mA·cm^{-2}. (d) Temperature differences.

water between the outlet and inlet was 1.05 °C at 500 mA·cm^{-2}, which increased to 2.22 °C at 1000 mA·cm^{-2} during the heating process. The corresponding heat transferred by the coolant water was approximately two times greater at 1000 mA·cm^{-2} than that at 500 mA·cm^{-2} under the same coolant water mass flow rate. Figure 5(d) shows the temperature differences between the maximum temperature in the stack and the coolant water increase with increasing current density. The temperature difference reached 19 °C during the cooling process at 1000 mA·cm^{-2}. This large difference and non-uniform temperature distribution would lead to unstable water phase change process and reduce the heat transfer capability of the coolant water. Clearly, the temperature difference of the coolant water fluctuated more during the heating process when the cooling system was closed. On the one hand, some of the liquid water that is generated may evaporate into vapor after the cooling process. On the other hand, part of the water vapor generated during the electrochemistry reaction can also be condensed into liquid because of large temperature difference between the single cell and the coolant water. In addition, as can be seen in Figure 5(b), although the temperature difference of the coolant water between the outlet and inlet increased from 1.22 °C to 1.7 °C, the heat removed by the coolant water decreased from 3900 W to 3500 W. As a result, the heat removal ability could be enhanced using the elevated convective heat transfer coefficient by increasing the coolant water mass flow rate.

4.4. Heat generation during the electrochemical reaction

The temporal profile of the mean voltage of the stack is shown in Figure 6(a). In the first 600 s, the voltage increased from 0.724 V to 0.745 V when the current density was maintained at 500 mA·cm^{-2}. The increase in voltage can be attributed to the dominant effect of catalyst activity on the cell voltage when the stack was heated [26]. Although the coolant water flow rates varied from 45 LPM to 30 LPM, the mean voltage of the stack was maintained at 0.734 V with the least standard deviation while the current density was 600 mA·cm^{-2}. During this process, the

PEMFCs operated steadily under high output efficiency. The mean voltage dropped to approximately 0.664 V when the current density increased to 1000 mA·cm^{-2}. The temperature within the cell increased rapidly due to the limited cooling ability of the coolant water, which also explained the reason why the cooling system was opened to control the operation temperature. Although the average voltage oscillated during the cooling and heating processes, the stack was still in high uniformity with a standard deviation less than 0.08.

The heat generation rate during the electrochemical reaction is displayed in Figure 6(b). The amount of generated heat increased with an increase of current density. Fortunately, it was always less than that removed by the coolant water in Figure 5. The difference between the generated and removed heat increased with the increase in current density. Moreover, the differences were 1400 W and 3000 W during the heating and cooling process at 1000 mA·cm^{-2}, respectively. Therefore, phase change played an important role in the heat balance, especially at high current density.

4.5. Heat balance analysis

As mentioned previously, phase change affects the cell performance and the heat removal capability of the coolant water. Figure 7(a) clearly illustrates the effect of phase change on the total heat removal. Without considering phase change, the thermal balance coefficients were all above the equilibrium line, indicating that heat removed by the coolant water was greater than the amount generated by the electrochemical reaction. Only 85% of the total heat was removed during the heating process with a coolant water flow rate of 45 LPM. A lower percentage would be caused by insufficient heat exchange with a decreased coolant water mass flow rate of 30 LPM. In addition, heat generated because of the phase change was approximately 40% of the heat removed by the coolant water, and the percentage decreased to approximately 33% when the stack was in a cooling process at a current density of 1000 mA·cm^{-2}.
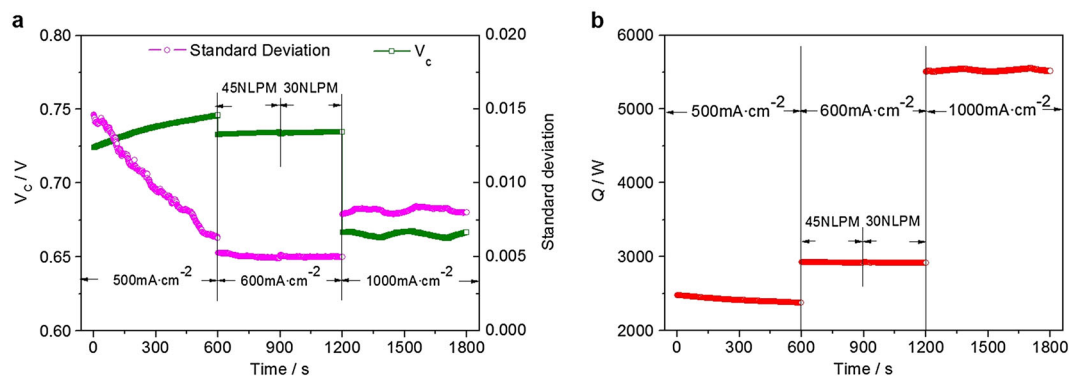
Figure 6. Heat generated during the electrochemical reaction. (a) Voltage evolution. (b) Electrochemical reaction heat evolution.
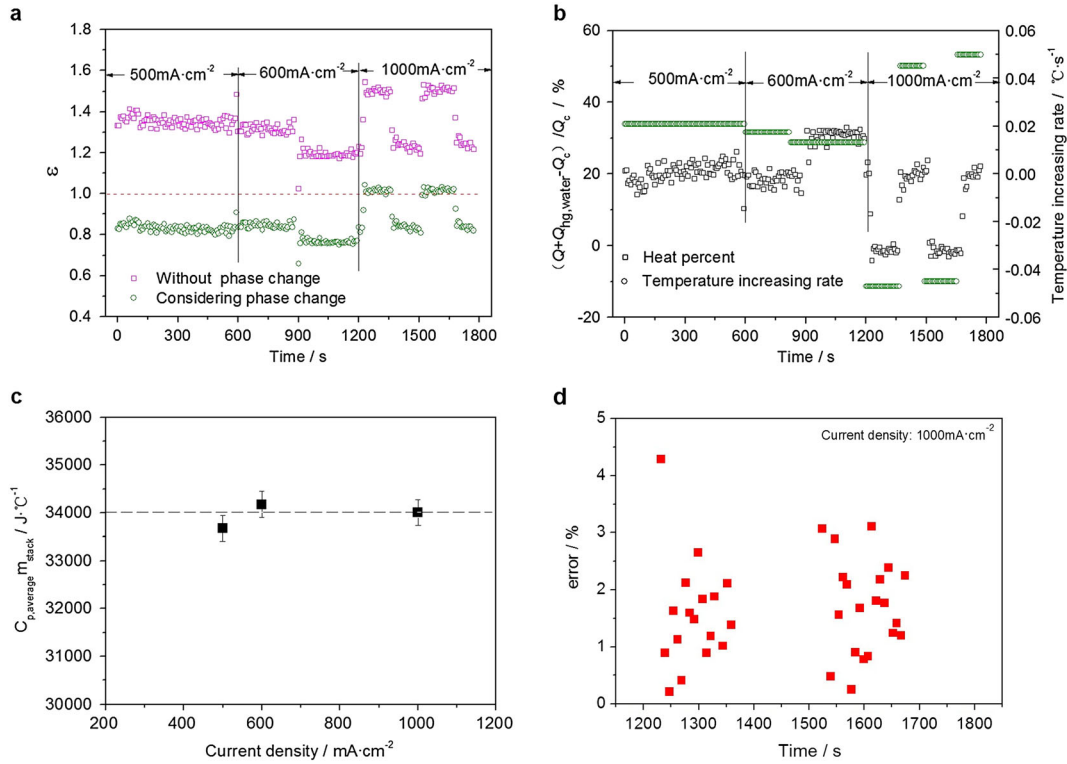
Figure 7. Heat balance in the stack. (a) Thermal balance coefficient. (b) Excess heat and rate of temperature increase in the stack. (c) Heat balance in the stack. (d) Error analysis.

Figure 7(b) shows the excess heat and its effect on the temperature increase rate in the stack. Nearly 20% of the heat removed by the coolant water at a coolant water flow rate of 45 LPM was used to heat the cooling system shown in Figure 1(b). Although the amount increased to 33% at 600 mA·cm^{-2}, when the coolant flow rate was decreased to 30 LPM, the rate of temperature increase was lower than that at 45 LPM, suggesting that less heat was removed by the coolant water at the decreased flow rate. During the cooling process at 1000 mA·cm^{-2}, that percentage decreased close to zero and the thermal balance coefficient reached unity, indicating that the heat generated in the stack was equal to the heat removed by the coolant water, resulting in heat balance in the stack. During the heating process, the heat balance could be also expressed as,

$$\Phi = \int_0^\tau Q_{excess} d\tau = \int_0^\tau (Q + Q_{hg,water} - Q_c) d\tau$$
$$= C_{p,average} m_{stack} \Delta t \qquad (12)$$

where Φ is the total amount of heat, Q_{excess} is the excess heat, τ is the operation time, Δt is the temperature increase at the heating process, and $C_{p,\ average}$ and m_{stack} are the specific heat capacity and mass of the stack in the system, respectively. Equation (12) can be rewritten as

$$C_{p,\ average} m_{stack} = \frac{(Q + Q_{hg,water} - Q_c)}{\frac{\Delta t}{\tau}}$$
$$= \frac{(Q + Q_{hg,water} - Q_c)}{\dot{t}} \qquad (13)$$

where $\dot{t}$ is the temperature increase rate of the stack system. In general, $C_{p,\ average}$ and m_{stack} are both physical properties of the stack itself in the system. In this case, $\frac{(Q + Q_{hg,water} - Q_c)}{\dot{t}}$ on the right-hand side of Eq. (13) is a constant during the heating process at different current densities. The specified values of $C_{p,\ average} m_{stack}$ under different cases are almost equal to 3.4×10^4 J °C^{-1} in Figure 7(c), indicating that the stack system was in good heat balance and the experimental data were well validated.

4.6. Error analysis

To calculate the error of the balance coefficient, Eq. (11) can be rewritten as:

$$y = \frac{1}{\varepsilon} = \frac{Q + Q_{hg,water}}{Q_c} \qquad (14)$$

$$= \frac{nI(1.25 - V_c) + \dot{m}_{l,H_2O} L_{H_2O}}{C_{l,water} \dot{m}_{water} (T_{water,out} - T_{water,in})}$$

where: $C_{i,water} = A$, $1.25nI + \dot{m}_{l,H_2O} L_{H_2O} = B$, $nI = C; \theta = T_{water,out} - T_{water,in}$. Eq. (14) can be simplified as,

$$y = \frac{1}{\varepsilon} = \frac{Q + Q_{hg,water}}{Q_c} = \frac{B}{A\dot{m}\theta} - \frac{CV_c}{A\dot{m}\theta} \qquad (15)$$

The absolute errors of the parameters are as follows,

$$\Delta\theta = 0.2, \quad \Delta V_c = 0.0001, \quad \Delta\dot{m} = 0.00002,$$

$$\Delta y = \left(-\frac{B}{A\dot{m}\theta^2} + \frac{CV_c}{A\dot{m}\theta^2} \right) \cdot \Delta\theta - \frac{C}{A\dot{m}\theta} \cdot \Delta V_c$$
$$- \left(\frac{B}{A\dot{m}^2\theta} - \frac{CV_c}{A\dot{m}^2\theta} \right) \cdot \Delta\dot{m} \qquad (16)$$

When the current density is $1000\,\text{mA·cm}^{-2}$,

$$\Delta y = \left(-\frac{B}{A\dot{m}\theta^2} + \frac{CV_c}{A\dot{m}\theta^2} \right) \cdot \Delta\theta - \frac{C}{A\dot{m}\theta} \cdot \Delta V_c$$
$$- \left(\frac{B}{A\dot{m}^2\theta} - \frac{CV_c}{A\dot{m}^2\theta} \right) \cdot \Delta\dot{m} = -0.08$$

Therefore, the absolute and relative errors of balance coefficient can be expressed as:

$$\Delta\varepsilon = \pm \left(-y^{-2} \cdot \Delta y \right) = \pm 0.08 \qquad (17)$$

$$\delta_\varepsilon = \frac{\Delta\varepsilon}{\varepsilon} \times 100\% = 8\% \qquad (18)$$

Furthermore, the relative errors of the parameters can be expressed as,

$$E_m = \frac{\Delta\dot{m}}{\dot{m}} = \frac{0.00002}{0.735} = 0.03\% \qquad (19)$$

$$E_\theta = \frac{\Delta\theta}{\theta} = \frac{0.2}{2.496} = 8\% \qquad (20)$$

$$E_{V_c} = \frac{\Delta V_C}{V_C} = \frac{0.0001}{0.6652} = 0.015\% \qquad (21)$$

Figure 7(d) shows the error analysis of balance coefficient at a current density of $1000\,\text{mA·cm}^{-2}$. It is clear that the heat removed by the coolant water is slightly greater than that generated in the fuel cell stack. In fact, the phenomenon will not occur according to the first law of thermodynamics. The reasons for this may include a measuring error of the coolant water inlet and outlet temperatures, the neglect of natural convection between the stack and the environment, and the experimental operating conditions. The experimental errors at all monitoring points were within 5%, which is an acceptable accuracy for experimental data analysis. The error is mainly attributed to instrumental error, including temperature, mass flow rate, and voltage measurements. The most serious factor is the accuracy of the temperature measurements. To improve the validity of the experiment, higher precision instruments should be used for the temperature measurements.

5. CONCLUSIONS

We investigated the phase change and its effect on the heat balance in a PEM stack both theoretically and experimentally. Conclusions can be drawn as follows:

- The theoretical analysis of phase change and its effect on the heat balance was successfully validated by its good agreement with the experimental data. The heat removed by the coolant water was more than that generated by the electrochemical reaction irrespective of the stack being in the heating or cooling process. The effect of the phase change on heat balance must be accounted for to yield reliable results.
- During the heating process, the heat removed by the coolant water was less than the total heat generated by the electrochemical reaction and phase change. The amount of heat removed by the coolant water can be enhanced by improving the convection heat transfer coefficient at an elevated coolant water flow rate.
- During the cooling process, all the heat generated in the stack can be removed by the coolant water and the thermal balance coefficient can reach 1.0. However, because of the large temperature difference between the MEA and the coolant water at high operating current density, a bipolar plate with high heat conductivity coefficient is required to improve temperature uniformity in the stack.
- Besides the thermal balance coefficient, the arithmetic product of the specific heat capacity and mass of the stack can be used as a novel criterion for the heat balance in asystem and the validation of the experimental data.

NOMENCLATURE

Q	= Electrochemistry reaction heat (W)
Q_{extra}	= Heat removed by the cooling system (W)
$\Delta\overline{h}_f$	= Enthalpy of formation (kJ·mol^{-1})
I	= Current density (A)
V_c	= Average voltage of the stack (V)
n	= Cell number
λ	= Stoichiometry
F	= Faraday constant (C·mol^{-1})
RH	= Relative humidity (%)
M_{H_2O}	= Water molecular weight (kg·mol^{-1})

$p_{a,inlet}$	= Inlet pressure at the anode (Pa)
$p_{c,inlet}$	= Inlet pressure at the cathode (Pa)
$T_{a,inlet}$	= Inlet temperature at the anode (°C)
$T_{c,inlet}$	= Inlet temperature at the cathode (°C)
$p_{sat}(T_{a,inlet})$	= Saturated water vapor pressure at the anode in the inlet (Pa)
$p_{sat}(T_{c,inlet})$	= Saturated water vapor pressure at the cathode in the inlet (Pa)
$p_{a,outlet}$	= Outlet pressure at the anode (Pa)
$p_{c,outlet}$	= Outlet pressure at the cathode (Pa)
$T_{a,outlet}$	= Outlet temperature at the anode (°C)
$T_{c,outlet}$	= Outlet temperature at the cathode (°C)
$p_{sat}(T_{a,outlet})$	= Saturated water vapor pressure at the anode in the outlet (Pa)
$p_{sat}(T_{c,outlet})$	= Saturated water vapor pressure at the cathode in the outlet (Pa)
$m_{a,add}$	= Water vapor mass flow rate at anode in the inlet (kg·s^{-1})
$m_{c,add}$	= Water vapor mass flow rate at cathode in the inlet (kg·s^{-1})
$m_{a,out}$	= Water vapor mass flow rate at anode in the outlet (kg·s^{-1})
$m_{c,out}$	= Water vapor mass flow rate at cathode in the outlet (kg·s^{-1})
m_{gen,H_2O}	= Water mass flow rate in the electrochemistry reaction (kg·s^{-1})
m_{l,H_2O}	= Liquid water mass flow rate generated in the stack (kg·s^{-1})
L_{H_2O}	= Latent heat of water (J·kg^{-1})
Q_c	= Heat removed by the coolant water (W)
$\dot{m}_{water}$	= Coolant water mass flow rate (kg·s^{-1})
$C_{l,water}$	= Specific heat of coolant water (J·kg^{-1}·°C^{-1})
$T_{coolant\ water,\ in}$	= Inlet temperature of the coolant water (°C)
$T_{coolant\ water,out}$	= Outlet temperature of the coolant water (°C)
$T_{coolant\ water,mean}$	= Mean coolant water temperature (°C)
$\Delta T_{max-mean}$	= Temperature difference between the maximum temperature in the cell and mean coolant water temperature (°C)
$\Delta T_{coolant\ water}$	= Temperature difference between the inlet and outlet coolant water (°C)
ε	= Thermal balance coefficient

Φ	= Heat amount (J)
Q_{excess}	= Excess heat (W)
τ	= Time (s)
i	= Temperature increasing rate (°C·s^{-1})
Δt	= Temperature increasing amount during the heating process (°C)
$C_{p,\ average}$	= Specific heat capacity of the stack (J·kg^{-1}·°C^{-1})
m_{stack}	= Mass of the stack in the system (kg)
$m_{inlet,\ H_2O(g)}$	= Total water vapor mass flow rate in the inlet (kg·s^{-1})
$m_{outlet,\ H_2O(g)}$	= Total water vapor mass flow rate in the outlet (kg·s^{-1})

ACKNOWLEDGEMENTS

REFERENCES

1. Williams MC. *Fuel Cell Handbook*, 7th ed. EG&G Technical Services Inc.: West Virginia, US Department of Energy, 2004.

2. Srinivasan S. *Fuel Cells: From Fundamentals to Applications*. Springer: Heidelberg, 2006.

3. Wang Y, Chen KS, Mishler J, Cho SC, Adroher XC. A review of polymer electrolyte membrane fuel cells: technology, applications, and needs on fundamental research. *Applied Energy* 2011; **88**:981–1007.

4. Barelli L, Bidini G, Ottaviano A. Optimization of a PEMFC/battery pack power system for a bus application. *Applied Energy* 2012; **91**(1):13–28.

5. Kandlikar SG, Lu Z. Thermal management issues in a PEMFC stack-A brief review of current status. *Applied Thermal Engineering* 2009; **29**:1276–1280.

6. Freire TJP, Gonzalez ER. Effect of membrane characteristics and humidification conditions on the impedance response of polymer electrolyte fuel cells. *Journal of Electroanalytical Chemistry* 2001; **503**:57–68.

7. Yi PY, Peng LF, Lai XM, *et al.* A Novel Design of Wave-Like PEMFC Stack with Undulate MEAs and Perforated Bipolar Plates. *Fuel Cells* 2010; **10**:111–117.

8. Wen CY, Huang GW. Application of a thermally conductive pyrolytic graphite sheet to thermal management of a PEM fuel cell. *Journal of Power Sources* 2008; **178**:132–140.

9. Tu ZK, Zhang HN, Luo ZP, *et al.* Evaluation of 5 kW Proton Exchange Membrane Fuel Cell Stack Operated at 95 °C under Ambient Pressure. *Journal of Power Sources* 2013; **222**:277–281.

10. Cao TF, Lin H, Chen L, He YL, Tao WQ. Numerical investigation of the coupled water and thermal management in PEM fuel cell. *Applied Energy* 2013; **112**:1115–25.

11. Wan ZM, Wan JH, Liu J, *et al.* Water recovery and air humidification by condensing the moisture in the outlet gas of a proton exchange membrane fuel cell stack. *Applied Thermal Engineering* 2012; **42**:173–178.

12. Yu Y, Tu ZK, Zhan ZG, *et al.* Gravity effect on the performance of PEM Fuel Cell Stack with different gas inlet/outlet positions. *International Journal of Energy Research* 2012; **36**(7):845–855.

13. Ramousse J, Lottin O, Didierjean S, *et al.* Heat sources in proton exchange membrane (PEM) fuel cells. *Journal of Power Sources* 2009; **192**:435–441.

14. Park JW, Jiao K, Li X. Numerical investigations on liquid water removal from the porous gas diffusion layer by reactant flow. *Applied Energy* 2010; **87**:2180–2186.

15. Jiao K, Park J, Li X. Experimental investigations on liquid water removal from the gas diffusion layer by reactant flow in a PEM fuel cell. *Applied Energy* 2010; **87**:2770–2777.

16. Zong Y, Zhou B, Sobiesiak A. Water and thermal management in a single PEM fuel cell with non-uniform stack temperature. *Journal of Power Sources* 2006; **161**:143–159.

17. Afshari E, Jazayeri SA, Barzi YM. Effect of water phase change on temperature distribution in proton exchange membrane fuel cells. *Heat and Mass Transfer* 2010; **46**:1295–1305.

18. Afshari E, Jazayeri SA. Effects of the cell thermal behavior and water phase change on a proton exchange membrane fuel cell performance. *Energy Conversion and Management* 2010; **51**:655–662.

19. Khajeh-Hosseini-Dalasm N, Fushinobu K, Okazaki K. Phase change in the cathode side of a proton exchange membrane fuel cell. *Journal of Power Sources* 2010; **195**:7003–7010.

20. Khajeh-Hosseini-Dalasm N, Fushinobu K, Okazaki K. Transient Phase Change in the Cathode Side of a PEM Fuel Cell. *Journal of the Electrochemical Society* 2010; **157**(10):B1358–B1369.

21. Jung CY, Shim HS, Koo SM, *et al.* Investigations of the temperature distribution in proton exchange membrane fuel cells. *Applied Energy* 2012; **93**:733–741.

22. Ju H, Meng H, Wang CH, *et al.* A single phase, non-isothermal model for PEM fuel cells. *International Journal of Heat and Mass Transfer* 2005; **48**:1303–1315.

23. Xue X, Tang J. PEM fuel cell dynamic model with phase change effect. *Transactions of the ASME: Journal of the Fuel Cell Science and Technology* 2005; **2**:274–283.

24. Kim YB. Study on the effect of humidity and stoichiometry on the water saturation of PEM fuel cells. *International Journal of Energy Research* 2011; **36**:509–522.

25. Abdul Rasheed RK, Ehteshami SMM, Chan SH. Analytical modelling of boiling phase change phenomenon in high-temperature proton exchange membrane fuel cells during warm-up process. *International Journal of Hydrogen Energy* 2014; **39**:2246–2260.

26. Gomatom P, Jewell W. Fuel parameter and quality constraints for fuel cell distributed generators. *Proceedings of the IEEE Conference and Exposition: Transmission and Distribution*, 2003; 409–412.

27. Nam JH, Kaviany M. Effective diffusivity and water-saturation distribution in single and two-layer PEMFC diffusion medium. *International Journal of Heat and Mass Transfer* 2003; **46**:4595–4611.

28. Larminie J, Dicks A. *Fuel cell systems explained*. John Willey & Sons Inc: New York, 2000.

29. Dai W, Wang HJ, Yuan XZ, *et al.* A review on water balance in the membrane electrode assembly of proton exchange membrane fuel cells. *International Journal of Hydrogen Energy* 2009; **34**(23):9461–9478.

30. Wan ZM, Liu J, Luo ZP, *et al.* Evaluation of self-water-removal in a dead-ended proton exchange membrane fuel cell. *Applied Energy* 2013; **104**:751–757.

31. Pei HC, Liu ZC, Zhang HN, *et al.* In situ measurement of temperature distribution in proton exchange membrane fuel cell I a hydrogen-air stack. *Journal of Power Sources* 2013; **227**:72–79.